ARTICLE

Quantum Chemistry Study on Local Structure and Properties of Amorphous $Fe_{80}P_{20}$ Alloy

Zhi-gang Fang*, Hong-zhi Hu, Jing-xue Guo, Qiu-ju Li

School of Chemical Engineering, Anshan University of Science and Technology, Anshan 114044, China

(Dated: Received on June 13, 2005; Accepted on August 25, 2005)

According to the structure features of $Fe_{80}P_{20}$, A series of clusters Fe_4P were designed and focused on studying the stability of local structure, charge distribution and chemical bond. Using the DFT method, energy and structure of Fe_4P clusters were optimized and analyzed. The computational results showed that the energy of cluster $1^{(2)}$ has the lowest energy, and the possibility of its existence in the $Fe_{80}P_{20}$ is high. Analyzing the transition states among the clusters, it was found that the clusters in the doublet state are more stable than those in the quartet state. The numbers of the Fe−P bond in the clusters play important roles in the cluster stability and electrons transfer properties. The more numbers of Fe−P bonds in the clusters, the higher the cluster stability, and the weaker the ability of P atom to get electron. The number of Fe atoms, which has bonding interactions with the P atom, is direct proportional to the average 3d orbit population of Fe atom. Basing on the orbital population, average magnetic moments of each Fe atom in the Fe_4P clusters were calculated, and they are all smaller than that of single metal Fe atom. This suggests that all Fe_4P clusters have soft magnetic property and they are expected to be perfect material for preparing soft magnetic apparatus.

Key words: Amorphous $Fe_{80}P_{20}$ alloy, Local structure, DFT, Cluster

I. INTRODUCTION

Researches on ferromagnetism material of amorphous alloys had attracted the scientists' interest because of their excellent soft magnetism with high magnetic conductivity, low spoilage, low coercive force, highly saturated intensity of magnetization, high Curie point and preferable stability factor so on [1-3]. For instance, transition metal-metalloid (TM-M) amorphous alloy were used as rigid core of transformer and transducer owing to the excellent magnetism, which is not with traditional magnetism materials. But the critical cooling rate (R_C) of forming Fe-based amorphous alloys is very fast, generally $R_C \geq 10^4$ K/s, which increased the difficulty in Fe-based amorphous alloys preparation. It is even more difficult to precede with the next step to characterize their geometry and electronic structure [4]. In recent years, amorphous alloys also gained the great attention as a new type of catalytic material. Hereinto, amorphous alloys Fe−P system appeared to have remarkable catalytic property in hydrogenation reactions [5]. Recently several literatures reported that amorphous alloys Fe−P showed high catalytic activity in hydrogenating desulfurization (HDS) and hydrogenating denitrification (HDN) reactions, which are important reactions in petroleum processing [6-8]. Therefore, it is with great practical significance to study amorphous Fe−P alloys.

Researches on amorphous Fe−P alloys have focused on preparation techniques and performance characterization because of the special structure properties that were called short-range order, long-rang disorder and thermodynamic metastability of the amorphous alloys [4,9,10]. There has been little literature on its geometry and electronic structure properties. The development of *ab initio* quantum chemistry and density function theory (DFT) can provide accurate computing results of moderate molecule. Moreover, with the exponential growth of the memory and speed of computational power in the past decade, it is now much easier to have in computational studies of complex chemical systems theoretically. It has been proven successfully that through utilizing appropriate cluster model methods to simulate the local structure of amorphous alloys perfectly, a series of structure and electronic properties have been obtained, and these results can be correlate to the properties of amorphous alloys to a certain extent [11-13].

Therefore, in the present work we shall use DFT calculation of Fe_4P as the model clusters to simulate the local structure of the familiar amorphous $Fe_{80}P_{20}$ alloy, since they have the same Fe/P ratio as $Fe_{80}P_{20}$. The stable structures of a series of Fe_4P were obtained and their properties is discussed. We believe that this study would enhance our understanding of the structure and electronic properties of amorphous $Fe_{80}P_{20}$ alloy.

II. MODEL AND METHOD

A. Model

The basic characteristics of amorphous alloys is its short-range order and long-rang disorder, which means that the atoms in the three-dimensional space are with topological disorder. There is no crystalline defects in amorphous alloys, such as crystal boundary, dislocation and aliquation. The atoms are joined to keep short-range order by chemical bond in the range of sev-

*Author to whom correspondence should be addressed. E-mail: Lnfzg@163.com

eral angstroms (0.1 nm), whose structures are similar to atomic clusters. The atoms in clusters are bonded strongly, but the interactions between clusters are weak.

The method of atomic cluster is an effective way to study the local structure of amorphous alloys [14]. A proper cluster can reflect the local structure of amorphous alloys, and it also embodies its crystalline symmetry in short range. The adulterations, defects and bonds in local structure can also be discussed and predicted theoretically.

According to the experimental data of the most familiar proportion of Fe−P amorphous alloy ($Fe_{80}P_{20}$) [4,15,16], Fe_4P clusters with square pyramid, triangle dipyramid, and plane pentagon structures were used. By exchanging spatial position of different atoms, twenty clusters model structures can be obtained.

B. Computational methods

Clusters with chosen structure were optimized with DFT in doublet and quartet states, respectively. Using Gaussian 98 program package, all the calculations were carried out with Pentium 350 personal computers. Calculation methods are the Beche's three-Parameter semi-empirical exchange function (B_3) [17] along with the Lee, Yang, and Parr correlation function (LYP) [18]. The 10-core electron of iron and phosphors were replaced by a relativistic effective core potential (RECP) generated by Hay and Wadt [19]. Namely, the 3s, 3p, 3d, 4s, 4p orbit of Fe atom and 3s, 3p, 3d orbit of P atom in concern were set to the Dunning/Huzinaga [20] double ξ Gaussian basis set. And the polarization function of the 3d orbit of atom P was set to ξ=0.6.

III. RESULTS AND DISCUSSION

A. Geometries and energies

The chosen stating configurations were optimized in doublet and quartet states respectively with density function theory (DFT) method. A series of stable Fe_4P clusters in doublet and quartet states were determined with real frequencies analysis. It is found that there are several groups with different energies, and there is little difference of geometries and energies for clusters in the same group. This indicates that the spans of Morse potential energy curves of the Fe_4P clusters are wide enough that different configurations fell into the same trap. Among configurations with the lowest energy in each group, there are three stable configurations in the doublet state ($1^{(2)}$, $2^{(2)}$, $3^{(2)}$), while there are two stable configurations in the quartet state ($1^{(4)}$, $2^{(4)}$).

The geometries and energy parameters of Fe_4P clusters were displayed in Fig.1 and Table I. The majorities of stable configurations of Fe_4P clusters are triangle dipyramids, and there is only one plane configuration in the doublet state. The configuration $1^{(2)}$ in the doublet state, whose energy is the lowest, is the most stable configuration in all clusters. Its geometry is triangle dipyramid with two metal Fe atoms and one metalloid

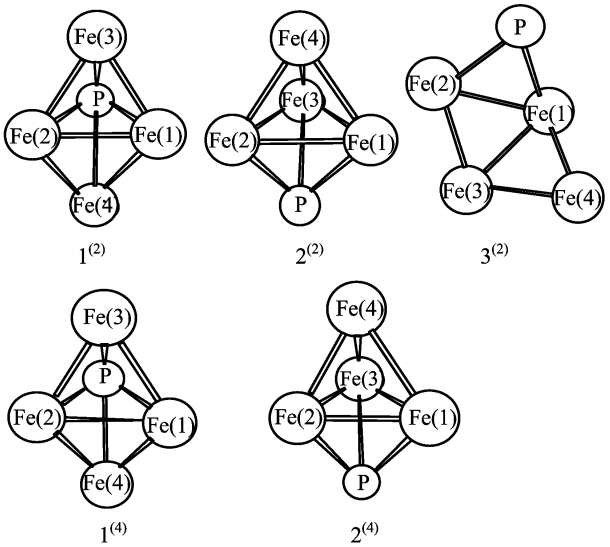

FIG. 1 Optimized structure of Fe_4P clusters with doublet and quartet states

TABLE I Energy parameters for Fe_4P cluster with doublet and quartet states

Cluster	Group	E_{ZPE}/a.u	E_{HOMO}/eV	E_{LUMO}/eV	ΔE/eV
$1^{(2)}$	C_{2V}	−500.2172	−4.5361	−2.4762	2.0599
$2^{(2)}$	C_1	−500.2109	−4.4082	−2.7211	1.6844
$3^{(2)}$	C_S	−500.1218	−4.6232	−3.2708	1.3524
$1^{(4)}$	C_{2V}	−500.1709	−4.6395	−2.6014	2.0354
$2^{(4)}$	C_{2V}	−500.1619	−4.5579	−2.8925	1.6653

P atom formed the central plane, and the other two Fe atoms on the two pyramid tops. The stable configuration with higher energy in the doublet state is configuration $2^{(2)}$, whose geometry is also triangle dipyramid. But the three metal Fe atoms are on the central plane, while one metal Fe and one metalloid P atom on the each of the two pyrimid tops. The stable configuration with highest energy in the doublet state is the plane configuration $3^{(2)}$. The geometries of configurations in the quartet state are similar to the ones in the doublet state with higher energies. Therefore, in the Fe_4P cluster, the stability in the doublet state is better than the ones in the quartet state with the same geometries. In summary, the $1^{(2)}$ cluster is with the lowest energy and most stable, which may well represent the local structure of amorphous $Fe_{80}P_{20}$ alloy. The gaps between HOMO and LUMO of configuration $1^{(2)}$, whose gap is the biggest, also point to the same conclusion.

The structure parameters of Fe_4P clusters in doublet and quartet states are listed in Table II. The bond lengths of Fe−P in the stable geometries of Fe_4P clusters varies in the range from 0.2281 to 0.2458 nm, and the bond length of Fe−Fe is from 0.2505 to 0.2792nm. These values are close to the experiment value of amorphous $Fe_{80}P_{20}$ alloy (Fe−P: 0.2460 nm, Fe−Fe: 0.2620nm) [15]. This indicates that Fe_4P is close to the local structure of amorphous $Fe_{80}P_{20}$ alloy. The average bond length of bond Fe−P and Fe−Fe in configuration $1^{(2)}$, whose energy is the lowest and is the

TABLE II Structure parameters for Fe_4P cluster with doublet and quartet state (Unit: nm)

Cluster	$R_{(Fe(1)-P)}$	$R_{(Fe(2)-P)}$	$R_{(Fe(3)-P)}$	$R_{(Fe(4)-P)}$	$R_{(Fe-P)}$	$R_{(Fe(1,2))}$	$R_{(Fe(1,3))}$	$R_{(Fe(1,4))}$	$R_{(Fe(2,3))}$	$R_{(Fe-Fe)}$
$Fe_{80}P_{20}$[a]					0.2460					0.2620
$Fe_{80}P_{20}$[b]					0.2440					0.2510
$1^{(2)}$	0.2394	0.2394	0.2396	0.2396	0.2395	0.2605	0.2602	0.2652	0.2652	0.2623
$2^{(2)}$	0.2290	0.2326	0.2356	0.3830	0.2324	0.2792	0.2688	0.2618	0.2598	0.2656
$3^{(2)}$	0.2297	0.2397	0.4687	0.4255	0.2347	0.2523	0.2448	0.2562	0.2640	0.2530
$1^{(4)}$	0.2285	0.2349	0.2458	0.2444	0.2384	0.2529	0.2627	0.2511	0.2538	0.2542
$2^{(4)}$	0.2281	0.2340	0.2330	0.3808	0.2317	0.2569	0.2755	0.2655	0.2655	0.2621

[a]$Fe_{80}P_{20}$ [15]: experimental value of $Fe_{80}P_{20}$.
[b]$Fe_{80}P_{20}$T [16]: theory value of $Fe_{80}P_{20}$ $R_{(Fe-P)}$: average bond length of Fe−P, $R_{(Fe-Fe)}$: average bond length of Fe−Fe

TABLE III Bond order of optimized structure for Fe_4P cluster in doublet and quartet states

Cluster	$Fe_{(1)}$−P	$Fe_{(2)}$−P	$Fe_{(3)}$−P	$Fe_{(4)}$−P	$Fe_{(1,2)}$	$Fe_{(1,3)}$	$Fe_{(1,4)}$	$Fe_{(2,3)}$	Fe−P%
$1^{(2)}$	0.2582	0.2582	0.1316	0.1316	0.0003	0.0423	0.0234	0.0234	80.65%
$2^{(2)}$	0.3366	0.2780	0.2444	−0.0478	−0.0576	−0.0267	0.0726	0.0472	81.72%
$3^{(2)}$	0.3061	0.2573	−0.0053	0.0091	0.1997	0.1590	0.0442	0.0509	47.47%
$1^{(4)}$	0.3148	0.2048	0.1503	0.1115	0.0444	0.0056	0.0503	0.0169	79.31%
$2^{(4)}$	0.3402	0.2599	0.2681	−0.0489	0.0552	−0.0563	0.0673	−0.0196	76.97%

Fe−P%: percentage of Fe−P bond order in Fe_4P clusters

most stable cluster in thermodynamics, is 0.2395 and 0.2623 nm respectively. These values of configuration $1^{(2)}$ Fe_4P cluster are the closest to the experiment values of amorphous $Fe_{80}P_{20}$ alloy among all the optimized clusters. the differences are only 6.5 and 0.3 pm for the two bonds, respectively. Therefore, configuration $1^{(2)}$ of Fe_4P cluster may be used to represent the local structure of amorphous $Fe_{80}P_{20}$ alloy.

The literature values of the bond length in amorphous $Fe_{80}P_{20}$ alloy obtained with the Non-Consistent LCAO experience models by Ching and Xu were listed in Table II [16]. In our results, the average bond length of Fe−P bond in Fe_4P clusters is in the range from 0.2317 to 0.2395 nm, and the difference from the experiment value is from 6.5 to 1.43 pm, which is slightly bigger than that in the literature (0.2 pm). The average bond lengths of Fe−Fe in Fe_4P clusters is from 0.2530 to 0.2656 nm and the difference from the experiment value is from 0.3 to 0.9 pm, which is smaller than that in the literature (11.0 pm). This may indicate that the models used in present paper may well represent the bonding between atoms in the amorphous alloy, and the simulations of bonding between transition metals (TM-TM) appear to be more accurate.

The fact that the bond length of Fe−P bond is shorter than the radius sum of atom iron and phosphor suggests stronger bonding between the atoms Fe and P, which is in agreement with previous literature [21]. The bigger values of the bond orders of the Fe−P bond in Table III support this conclusion. Except for the plane configuration $3^{(2)}$, the bond orders of the Fe−Fe bond in the Fe_4P clusters are relatively very small. Some of the values are even negative, which may suggest formation of anti-bond. Therefore, the interactions between Fe atoms are not strong. The percentages of the Fe−P bond in Fe_4P clusters are in the range from 76.97% to 81.72%. This indicates that Fe−P bond is the primary reason for the stability of the cluster.

B. Thermodynamics properties

Fe_4 cluster was computed with same calculation level (B3LYP/Lanl2dz). After energy minimization and frequency analysis, the structure with the most stable geometry and energy was obtained. We assume that the cluster growth pathway of Fe_4P is through P atom addition to cluster Fe_4, i.e. as the following reaction:

$$Fe_4+P \rightarrow Fe_4P \quad (1)$$

Optimized energy and Gibbs free energy of cluster Fe_4 and single point energy and Gibbs free energy of atom P were listed in Table IV. The binding energies (E_{BE}) and the change of Gibbs free energies (ΔG) of clusters Fe_4P in the growth pathway were calculated according to $E_{BE} = E_{Fe_4} + E_P - E_{Fe_4P}$, and $\Delta G = G_{Fe_4P} - G_{Fe_4} - G_P$.

The change of Gibbs free energies determines the direction of the reaction. The binding energy determines the stability of clusters. The higher the binding energy, the easier for the cluster growth. For the isomers of cluster Fe_4P, the binding energies are positive and the changes of Gibbs free energies are negative, and their absolute values are quite significant. Therefore, all the isomers should be stable, and the configuration $1^{(2)}$ structure is the stablest.

TABLE IV Corrected energy(E_{ZPE}), binding energy(E_{BE}), G and ΔG for clusters Fe_4P

Cluster	E_{ZPE}/a.u	E_{BE}/a.u	G/a.u	ΔG/a.u
Fe_4	−493.6338		−493.6698	
P	−6.3555		−6.4381	
$1^{(2)}$	−500.2172	0.2279	−500.2540	−0.1460
$2^{(2)}$	−500.2109	0.2216	−500.2482	−0.1402
$3^{(2)}$	−500.1218	0.1325	−500.1599	−0.0519
$1^{(4)}$	−500.1709	0.1816	−500.2163	−0.1083
$2^{(4)}$	−500.1619	0.1726	−500.2079	−0.0999

C. Transition states

Transitions between different Fe_4P configurations each cluster were calculated using QST2 methods under with same computing level (B3LYP/Lanl2dz). There are only four transition states ($2^{(2)}\rightarrow1^{(2)}$, $1^{(4)}\rightarrow2^{(2)}$, $2^{(4)}\rightarrow1^{(4)}$, $3^{(2)}\rightarrow2^{(4)}$) were obtained in finding whose energies are higher than the two cluster isomers and whose frequency has only a single negative value(Table V). The transitions and potential energies of cluster Fe_4P were plotted in Figure 2.

TABLE V Transition state energy (E_{TS}), energy barrier (E_A, E_B) between isomers for cluster Fe_4P

Reaction	E_{TS}/a.u	E_A/a.u	E_B/a.u
$3^{(2)}\rightarrow2^{(4)}$	−500.1041	0.0177	0.0578
$2^{(4)}\rightarrow1^{(4)}$	−500.1620	0.0001	0.0089
$1^{(4)}\rightarrow2^{(2)}$	−500.1698	0.0009	0.0411
$2^{(2)}\rightarrow1^{(2)}$	−500.2063	0.0046	0.0109

E_A: the forward react energy barrier, E_B: the backward react energy barrier.

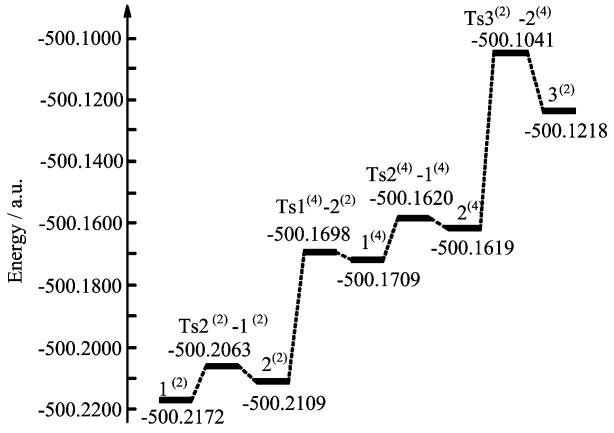

FIG. 2 The energy diagram of cluster Fe_4P and their transitions

It is interesting that the transition state can only exist between the configurations with adjacent energies. When the isomers make the transition from higher energy quartet state to lower one, the activation energies are relatively small. The activation energies of their inverse reactions are much larger correspondingly. Therefore, the configurations in the quartet state are relatively unstable, and they can easily change into to one configuration in the doublet state. Configuration $3^{(2)}$ has the highest energy among these cluster configurations, but the activation energy from configuration $3^{(2)}$ to $2^{(4)}$ is high, and it is difficult to take place. Generally speaking, the stability in doublet state is better than the one in quartet state. Therefore, it is more likely that Fe_4P cluster in the doublet state may represent the structure of amorphous $Fe_{80}P_{20}$ alloy.

D. Electronic properties

The atomic distribution of electrons in Fe_4P cluster is displayed in Table VI. It appears that the direction of electron transfer of P atoms in clusters does not follow any certain rules. It occurs both ways: from metal to metalloid and form metalloid to metal. It was suggested that this is related to the number of metal atoms around the P atom [22]. In configuration $1^{(2)}$ and $1^{(4)}$, there are bonding interactions between the four Fe atoms and P atom, respectively. The P atoms has positive charges because of losing electrons (0.0536, 0.0904). In configurations $2^{(2)}$ and $2^{(4)}$, the atoms P has negative charges because of gaining electrons, however, the amount of electron transfer is small (−0.0067, −0.0006). In configurations $3^{(2)}$, P atom is bonded with two metal atoms, and the amount of electron transfer is much larger (−0.0322).

Either from the first ionization energies of atoms (P: 1011.8 MJ/mol, Fe: 759.4 MJ/mol) or the electronegativity (P: 2.05, Fe: 1.80), the metalloid P atom should have better ability to gain electron than metal Fe atom. However, in the local structure of amorphous alloys, the electron transfer of a certain atom is not determined by only pair interactions. So the direction of electron transfer can not be simply described with the first ionization energy and electronegativity, Rather, the local structure of the amorphous alloys as a whole determines it. Therefore, the bonding modes in the amorphous $Fe_{80}P_{20}$ alloy must have played an important role in the direction of electron transfer.

Further more, in order to make clear the microscopic electron transfer directions between atoms Fe and P, we listed the Mulliken orbital population of atom Fe and P of Fe_4P cluster in Table VI. Comparing with the orbital population of cluster Fe_4 and atom P (Fe $3d^{6.73}4s^{0.97}4p^{0.30}$, P $3s^{2.0}3p^{3.0}3d^{0.0}$), the Mulliken orbital population changes of each atom were obtained.

In Table VI, the average 3d orbits population of Fe atoms in the Fe_4P clusters increases, whose change ranges from 0.05 to 0.14. This may be interpreted [23] as the following. In the polyatomic clusters, the 4s orbits would expand, and the 4s electrons could drop into 3d orbits. This can decrease the cavities of the 3d orbits and their ferromagneticity, consequently the system becomes soft magnetic. This is consistent with the result that the average 4s orbits populations of Fe atoms become smaller, and the change ranges from −0.07 to

TABLE VI Mulliken charge, orbital population and population change of Fe and P in cluster Fe_4P

	Mulliken charge				
Cluster	Fe (1)	Fe (2)	Fe (3)	Fe (4)	P
$1^{(2)}$	0.0535	0.0535	−0.0803	−0.0803	0.0536
$2^{(2)}$	−0.0109	0.0098	0.0422	−0.0344	−0.0067
$3^{(2)}$	−0.0692	0.0648	−0.1072	0.1438	−0.0322
$1^{(4)}$	−0.0752	0.0253	−0.1023	0.0618	0.0904
$2^{(4)}$	−0.0032	0.0252	0.0051	−0.0265	−0.0006

	Mulliken orbital population and change											
	Fe/n			ΔFe/n			P			ΔP		
Cluster	3d	4s	4p	Δ3d	Δ4s	Δ4p	3s	3p	3d	Δ3s	Δ3p	Δ3d
$1^{(2)}$	6.84	0.86	0.32	0.11	−0.11	0.02	1.77	3.13	0.04	−0.23	0.13	0.04
$2^{(2)}$	6.80	0.90	0.30	0.07	−0.07	0.00	1.79	3.18	0.04	−0.21	0.18	0.04
$3^{(2)}$	6.78	0.85	0.37	0.05	−0.12	0.07	1.85	3.16	0.02	−0.15	0.16	0.02
$1^{(4)}$	6.87	0.84	0.31	0.14	−0.13	0.01	1.78	3.09	0.04	−0.22	0.09	0.04
$2^{(4)}$	6.83	0.87	0.31	0.10	−0.10	0.01	1.79	3.17	0.04	−0.21	0.17	0.04

Δd(Fe, P)=d(Fe_4P)-d(Fe_4, P), Δs(Fe, P)=s(Fe_4P)-s(Fe_4, P), Δp(Fe, P)=p(Fe_4P)−P(Fe_4, P). Fe/ n: average 3d orbital population of atom Fe

−0.13. The 3s and 3p orbits of the P atoms also changed apparently. The populations of 3s orbits decreased, and the change ranges from −0.15 to −0.23; the populations of 3p orbits increased, and the change ranges from 0.09 to 0.18. And the average 4p orbits populations of the Fe atoms and 3d orbits populations of the P atoms changed little. In summary, the 3d, 4s orbit of Fe atoms and the 3s, 3p orbit of the P atoms have more influence on the electron transfer and they play important roles in the stability of cluster Fe_4P.

There are some relations between the Mulliken population of atoms and the cluster geometries. When there is more bonding interaction among the Fe and P atoms in the clusters, there is more change of average 3d orbits populations of the Fe atoms. In configurations $1^{(2)}$ and $1^{(4)}$, which have four Fe atoms with bonding interaction with the P atoms, the changes of average 3d orbits populations of the Fe atoms are 0.11 and 0.14 respectively. In configurations $2^{(2)}$ and $2^{(4)}$, which have three Fe atoms with bonding interaction with the P atoms, the changes of average 3d orbits populations of the Fe atoms are 0.07 and 0.10 respectively. There are only two Fe atoms with bonding interaction with the P atoms in configuration $3^{(2)}$, and the 3d average orbits populations increase by 0.05. The average 3s orbits populations of the atom are also related to the quantity of Fe−P bond, viz. the more Fe−P bonding interaction, the bigger of the changes.

E. Magnetic properties

There were several reports on the relation between the magnetic moment and the components of amorphous alloys, especially for amorphous alloys that consist of transition metal Fe and metalloid B, Si, C and P [4,24,25]. Here the the magnetic properties of atoms were studied based on the study of the average 3d populations of the Fe atoms in Fe_4P clusters. The maganetic properties are determined by the 3d orbits populations and cavities of ferromagnetism metal. Therefore, the average cavities (N) of the Fe atoms in the clusters were calculated using the expression $\mu_s = \sqrt{N(N+2)}$, the average magnetic moment of each Fe atom in the clusters is obtained (see Table VII).

TABLE VII Average 3d population, cavity (N), and magnetic moment(μ_s) of Fe atom in Fe_4P

Cluster	3d/n	N	μ_s/BM
Fe_4	6.73	3.27	4.1513
$1^{(2)}$	6.84	3.17	4.0432
$2^{(2)}$	6.80	3.21	4.0844
$3^{(2)}$	6.78	3.22	4.0998
$1^{(4)}$	6.87	3.13	4.0071
$2^{(4)}$	6.83	3.18	4.0535

Figure 3 showed the average magnetic moment of the Fe atoms in the Fe_4P clusters. Because of the relation between the 3d orbits populations and geometries, the geometries also have effects on the average magnetic moment of each Fe atom in the clusters. The more metal Fe atoms have bonding interactions with the P atom, the smaller the magnetic moment. The average magnetic moment calculated is less than that of single atom Fe (4.8990 BM as calculated and 5.7−6.0 BM experimental) [26], and all of the clusters have soft magnetism. Configuration $3^{(2)}$ has the biggest magnetic moment, and the magnetic moment of configurations $1^{(2)}$ and $1^{(4)}$ are smaller. Since configuration $1^{(2)}$ has the lowest energy and highest stability, it the best as magnetic material.

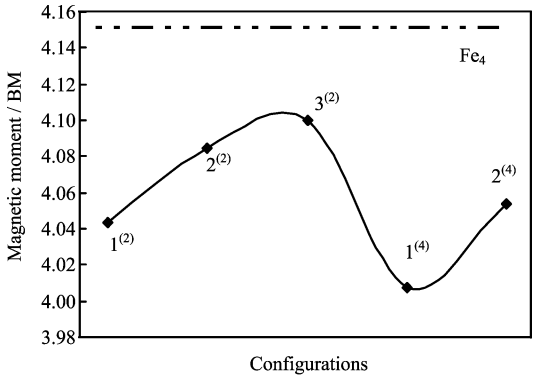

FIG. 3 Average magnetic moment of single Fe atom in Fe_4P clusters

IV. CONCLUSIONS

We used cluster models to simulate the local structure of amorphous $Fe_{80}P_{20}$ alloy. The square pyramid, triangle dipyramid, and plane pentagon configurations of Fe_4P cluster were chosen. After DFT energy optimizztion and frequency analysis, five stable configurations were obtained. Configuration $1^{(2)}$ has better stability and it can exist more easily in amorphous alloys. The bond lengths of the optimized configurations of Fe_4P cluster are close to those from the experiment data of amorphous $Fe_{80}P_{20}$ alloy. Among all the optimized cluster configurations, configuration $1^{(2)}$ of the Fe_4P clusters has the closest properties to the amorphous $Fe_{80}P_{20}$ alloy. Therefore, it is more likely that configuration $1^{(2)}$ reflects the local structure of amorphous $Fe_{80}P_{20}$ alloy. Computation of the transition states properties indicated that the stability in doublet state is better than that of the quartet state.

The number of Fe−P bond in the clusters plays an important role on the stability and electrons transfer property of the Fe_4P cluster. The more Fe−P bond numbers, the higher cluster stability, and the weaker ability of the P atom to get electrons. The number of Fe atom that bonded with the P atom, is directly proportional to the average 3d orbit population of the Fe atom. The average magnetic moment of Fe atoms in the Fe_4P clusters calculated is lower than that in single metal Fe atom. This suggests that all Fe_4P clusters can possess soft magnetic property, and they are expected to be the perfect material for preparing soft magnetic apparatus.

V. ACKNOWLEDGMENT

This work was supported by Anshan University of Science and Technology Research Project(No. 2003001).

[1] A. Garcia-Arribas, M. L. Fdez-Gubieda and J. M. Baradiarán, Phys. Rev. B **61**, 6238 (2000).
[2] R. Nakatani, M. Yamamoto and H. Yakame, J. Magn. Magn. Mate. **239**, 231 (2002).
[3] Y. Yamaguchi, K. Horiguchi and Y. Shindo, Adv. Cry. Eng. **43**, 469 (2003).
[4] F. E. Luborsky, *Amorphous Metallic Alloys*, C. Ke Trans., Beijing, Metallurgy Press (Yejin Chubanshe), (1989).
[5] G. C. Bond, Translated by P. Li, *Heterogeneous Catalysis*: *Principles and Applications*, Beijing: Beijing Press, (1982).
[6] A. R. José, Y. K. Jae and C. H. Jonathan, J. Phys. Chem. B **107**, 6276 (2003).
[7] X. W. Wang, P. Clark and S. T. Oyama, J. Catal. **208**, 321 (2002).
[8] P. Clark, W. Li and S. T. Oyama, J. Catal. **200**, 140 (2001).
[9] T. D. Shen, Y. He and R. B. Schwarz, J. Mater. Res. **14**, 2107 (1999).
[10] A. Böhönyey and G. Huhn, L. F. Kiss, J. Non-Crys. **232**, 490 (1998).
[11] Z. G. Fang, B. R. Shen and K. N. Fan, Chin. J. Chem. Phys. **15**, 17 (2002).
[12] Z. G. Fang, D. J. Liu and K. N. Fan, Chin. J. Chem. Phys. **17**, 684 (2004).
[13] Y. X. Chi, S. X. Tian and K. Z. Xu, Chin. J. Chem. Phys. **15**, 22 (2002).
[14] X. Lu, X. Xu , N. Wang and Q. Zhang, Chem. Phys Lett. **292**, 445 (1998).
[15] C. Hausleitner and Hafner, J. Phys. Rev. **47**, 5689 (1993).
[16] W. Y. Ching and Y. N. Xu, J. Appl. Phys. **70**, 6305 (1991).
[17] A. J. Beck, Chem. Phys. **98**, 5648 (1993).
[18] C. Lee, W. Yang and R. G. Parr, Phys. Rev. B **37**, 785 (1988).
[19] P. J. Hay, W. R. Walt and J. Chem. Phys. **82**, 270 (1985).
[20] T. H. Dunning and P. J. Hay, *Modern Theoretical Chemistry*, Vol. 3. New York: Plenum, (1977).
[21] R. P. Messmer, Phys Rev. B **23**, 1616 (1981).
[22] T. Imanaka, J. Tamaki and S. Teranishi, Chem. Lett. **164**, 449 (1984).
[23] Y. Wu, *Catalytic Chemistry*, Beijing; Science Press, (1998).
[24] J. Namkung, K. C. Kim and C. G. Park, Mate. Sci. Engi. **375-377**, 1116 (2004).
[25] H. Y. Zhao, S. W. Yao and W. G. Zhang, Chin. J. Chem. Phys. **17**, 752 (2004).
[26] Z. G. Xu, Q. R. Cai and Q. E. Zhang, *Modern Ligand Chemistry*, Beijing: Beijing Industry Press, (1987).